Microscopic observation of two-level systems in a metallic glass model (F)

(ID) Felix C. Mocanu, (ID) Ludovic Berthier, (ID) Simone Ciarella, et al.

COLLECTIONS

(F) This paper was selected as Featured

ARTICLES YOU MAY BE INTERESTED IN

Free energy calculations and unbiased molecular dynamics targeting the liquid–liquid transition in water no man's land
The Journal of Chemical Physics **158**, 014502 (2023); https://doi.org/10.1063/5.0120789

Weighted ensemble: Recent mathematical developments
The Journal of Chemical Physics **158**, 014108 (2023); https://doi.org/10.1063/5.0110873

Compact and complete description of non-Markovian dynamics
The Journal of Chemical Physics **158**, 014105 (2023); https://doi.org/10.1063/5.0132614

Microscopic observation of two-level systems in a metallic glass model Ⓕ

View Online   Export Citation   CrossMark

Felix C. Mocanu,[1,a)] ⓘD   Ludovic Berthier,[2,3] ⓘD   Simone Ciarella,[1] ⓘD   Dmytro Khomenko,[4,5] ⓘD
David R. Reichman,[4] ⓘD   Camille Scalliet,[6] ⓘD   and Francesco Zamponi[1] ⓘD

AFFILIATIONS

[1] Laboratoire de Physique de l'École Normale Supérieure, ENS, Université PSL, CNRS, Sorbonne Université, Université de Paris, 75005 Paris, France
[2] Yusuf Hamied Department of Chemistry, University of Cambridge, Lensfield Road, Cambridge CB2 1EW, United Kingdom
[3] Laboratoire Charles Coulomb (L2C), Université de Montpellier, CNRS, 34095 Montpellier, France
[4] Department of Chemistry, Columbia University, 3000 Broadway, New York, New York 10027, USA
[5] Dipartimento di Fisica, Sapienza Università di Roma, P.le A. Moro 2, I-00185 Rome, Italy
[6] DAMTP, Centre for Mathematical Sciences, University of Cambridge, Wilberforce Road, Cambridge CB3 0WA, United Kingdom

[a)]Author to whom correspondence should be addressed: felix-cosmin.mocanu@phys.ens.fr

ABSTRACT

The low-temperature quasi-universal behavior of amorphous solids has been attributed to the existence of spatially localized tunneling defects found in the low-energy regions of the potential energy landscape. Computational models of glasses can be studied to elucidate the microscopic nature of these defects. Recent simulation work has demonstrated the means of generating stable glassy configurations for models that mimic metallic glasses using the swap Monte Carlo algorithm. Building on these studies, we present an extensive exploration of the glassy metabasins of the potential energy landscape of a variant of the most widely used model of metallic glasses. We carefully identify tunneling defects and reveal their depletion with increased glass stability. The density of tunneling defects near the experimental glass transition temperature appears to be in good agreement with experimental measurements.

Published under an exclusive license by AIP Publishing. https://doi.org/10.1063/5.0128820

I. INTRODUCTION

The mechanical and thermal properties of glassy systems at cryogenic temperatures are determined by their low-energy excitations. In particular, at temperatures below 1 K, where quantum effects are important, the model of tunneling two-level systems (TLSs)[1,2] and its extensions[3] has proven to be remarkably successful in the prediction of the linear dependence in temperature T of the specific heat, the T^2 dependence of the thermal conductivity,[4,5] and the plateau in ultrasonic sound attenuation.[6,7] Despite its success, alternative explanations for these experimental observations have been proposed.[8,9] In particular, the interactions between TLS,[10] aspects related to the scattering of phonons by TLS,[11–14] and the collective TLS dynamics[15] remain the subject of debate.[16] Computational models can, in principle, be used to establish the relative merits and the ultimate validity of different hypotheses.[17–22]

Beyond answering fundamental questions about the glassy state, the existence and nature of low-energy excitations in non-crystalline solids are of significant practical interest as well. In the case of superconducting circuits used for quantum computation, the tunneling TLS present in the amorphous dielectric layers of these devices is thought to be a major source of noise and decoherence.[23] Similarly, the relationship of TLS defects to internal friction is an important factor for reducing the optical losses in the coatings used for glass mirrors that are part of the complex assemblies of gravitational wave detectors.[24,25]

A particularly important question is what controls the density of TLS, which, in turn, determines the thermal and transport properties of the glass. Previous work has identified the fictive temperature (T_f), which is "the temperature at which the glass sample would find itself in equilibrium if suddenly brought there from a given state"[26] and thus efficiently encodes the thermal history of the

glass, its stability, and position in the potential energy landscape, as a crucial determinant of the TLS density. In fact, a reduction of roughly two orders of magnitude was observed in experiments on evaporated silicon thin films,[27] on vapor-deposited indomethacin,[28] and in numerical simulations of polydisperse soft-spheres (PSSs),[21] where T_f was decreased from above (hyperquenched glass) to below (ultrastable glass) the experimental glass transition temperature T_g.

However, the numerical results for continuously polydisperse systems[21] indicate a TLS density significantly larger than experiments, which suggests that other parameters might be relevant in its determination. Here, we address this question by taking advantage of a recent extension of the swap Monte Carlo (MC) algorithm[29,30] to computer models of metallic glasses,[31] which feature both a reduced polydispersity and more realistic attractive interactions. We find the same reduction of the TLS density as a function of T_f as in previous work. In addition, we find an overall depletion with respect to previous simulations of highly polydisperse soft spheres. Our work thus suggests that the use of a more realistic yet relatively simple model is sufficient to bring down the absolute density of TLS, in closer agreement with experimental measurements of typical materials.[2,32] The TLS density is not a strongly universal quantity, being determined by both the microscopic parameters of the interaction potentials and the thermal history of the specific glass sample. Physically, our results confirm that increasing the glass stability considerably decreases the density of TLS, thus leading to an expected decrease in dissipation in amorphous solids at low temperatures and a concomitant improvement in the material attributes associated with a variety of practical applications.

Finally, we revisit previous numerical protocols for TLS determination[21] and provide a detailed insight on how the measured density of TLS depends on the exploration protocol and on the properties of energy minima and barriers inside glass metabasins. Finally, we investigate the glass vibrational modes in order to analyze the low-frequency quasi-localized modes (QLMs) found at the harmonic level. We find a weak correlation between the density of QLM and TLS, distinct from the proportionality suggested recently.[33] Our results emphasize the diversity of low-energy excitations governing the behavior of glasses at low and cryogenic temperatures.

Our article is organized as follows. In Sec. II, we present the numerical tools used to isolate and observe TLS. In Sec. III, we describe the results of the potential energy landscape exploration. In Sec. IV, we characterize the statistical properties of the TLSs and their temperature evolution. We discuss our results in Sec. V.

II. NUMERICAL METHODS

A. General strategy

Our ultimate goal is to numerically detect and characterize TLSs in a model metallic glass and investigate how their number and properties evolve with glass preparation. In experiments, TLSs are naturally excited at low temperature where quantum effects become relevant. However, simulating the quantum dynamics of glasses containing thousands of particles at very low temperature is prohibitively difficult, and one should find alternative approaches to identify TLSs.

Our aim is, therefore, to estimate $n(E)$, i.e., the number of tunneling double-well (DW) potentials (transition paths connecting distinct potential energy minima) with the associated quantum

splitting smaller than E, counted per atom and per glass sample. The TLS model[1,2] postulates the small-E scaling,

$$n(E) \simeq n_0 E + O(E^2). \tag{1}$$

The plateau value n_0 reached by $n(E)/E$ at small E allows one to estimate n_{TLS}, the number of active TLSs per atom in a typical glass sample at temperature T_Q where experiments are performed, typically around 1 K,

$$n_{TLS} = n_0 k_B T_Q. \tag{2}$$

The quantity n_{TLS} deduced from $n(E)$ from Eqs. (1) and (2) is the key factor controlling physical properties at low temperatures.

We provide a brief summary of our numerical strategy to measure $n(E)$ for glasses characterized by various fictive temperatures, while more detailed explanations and analysis will be presented in Sec. II-IV. There are four important steps:

1. Prepare glass samples of various degrees of stability or fictive temperatures. To do so, we generate N_g independent equilibrium configurations in the supercooled liquid phase at different temperatures T_f ranging from the mode-coupling crossover temperature T_{mct} down to the experimental glass transition temperature T_g using the swap Monte Carlo algorithm.[29] We then form glasses by rapidly quenching the configurations to a lower "exploration" temperature T_{exp} using conventional molecular dynamics (MD). Therefore, our glassy states at T_{exp} would correspond to equilibrium supercooled liquid configurations if brought back to T_f, which allows us to identify T_f with Tool's fictive temperature.[26] Varying T_f is similar to varying the cooling or deposition rate in experiments. Each of the N_g swap-generated equilibrium configurations defines a "glass sample" or a "glass metabasin."

2. Explore using MD the potential energy landscape of each glass metabasin,[34,35] which contains multiple potential energy minima, or inherent structures (ISs),[36–38] separated by energy barriers. The low exploration temperature T_{exp} is chosen to completely suppress particle diffusion over the simulated timescales, thus confining the exploration to a single glass metabasin defined by the initial configuration. At regular intervals during the dynamical trajectory simulated at T_{exp}, the potential energy is minimized to generate inherent structures. We call n_{IS} the number of distinct IS sampled over a single glass metabasin and N_{IS} that sampled over all N_g glasses.

3. The pairs of inherent structures visited consecutively in the trajectory are candidate double-well (DW) potentials if the transition is observed at least once in both directions. For those, we compute the minimum-energy path (MEP) connecting these pairs of ISs using the nudged elastic band (NEB) method.[39,40] We obtain a library of N_{DW} double-well potentials.

4. The minimum energy path provides an effective one-dimensional energy profile with two minima along which the quantum splitting, decay rate, and tunneling matrix elements are estimated via a one-dimensional Schrödinger equation.[17,21] We call $N_{DW}(E)$ the total number of double wells with a quantum splitting lower than E, with

$N_{DW}(E \to \infty) = N_{DW}$. The quantity $N_{DW}(E \sim k_B T_Q)$ is directly related to the number of two-level systems in the glass we wish to estimate.

It is useful to decompose the number $n(E)$ of low-energy excitations per atom and per glass sample as

$$n(E) = \frac{N_{DW}(E)}{N\, N_g} = \frac{1}{N} \times \frac{N_{IS}}{N_g} \times \frac{N_{DW}}{N_{IS}} \times \frac{N_{DW}(E)}{N_{DW}}, \quad (3)$$

where N is the number of atoms. The standard TLS model postulates that DW potentials originate from strongly localized atomic motions with a small, finite density. The number of DWs in a glass is thus extensive, yielding a finite $n(E)$. Physically, in order to be active at a given temperature T_Q over an observation time t_w, the TLS needs to have not only the relevant energy splitting $E \sim k_B T_Q$ but also a tunneling rate Γ such that $\Gamma t_w \gg 1$. Because the TLS model postulates a flat distribution of $\log \Gamma$ at small Γ, the effective number of active TLS grows as $\log t_w$ at large t_w.[1,2,41] In summary, according to the TLS model, we should expect a finite $n(E) \propto k_B T_Q \log t_w$ when N and N_g both diverge.

Given that our TLS detection protocol is different from the experimental one, we need to discuss how each ratio in Eq. (3) is expected to behave when its denominator diverges, i.e., when we increase statistics. Let us first consider the ratio $N_{DW}(E)/N_{DW}$. This is the cumulative histogram of quantum splittings, which then converges to a finite limit when $N_{DW} \to \infty$. The TLS model then predicts that the remaining ratio $N_{DW}/(N_g \times N)$ converges to a finite value for large N and N_{IS}. However, we discuss in Appendix A that this ratio, as measured in our numerical protocol, may have very different behaviors depending on the nature of TLS and their interactions. In particular, because we work at fixed (and not very large) N and because the N_g glass samples are independent, the total number of sampled IS scales as $N_{IS} \propto N_g$ and the ratio N_{IS}/N_g then converges to a finite value when $N_g \to \infty$ at finite N. However, as we will see, this value is so large (naturally scaling as $\exp N$) that we are not able to enumerate all the IS in a reasonable exploration time, and as a result, N_{IS}/N_g depends (albeit quite weakly) on exploration time in the classical MD simulation at temperature T_{exp}. Predicting the large scale behavior of N_{DW}/N_{IS} is more intricate; see Appendix A for a discussion; we observe in our exploration protocol that this ratio remains of order one and depends very weakly on the chosen exploration time.

Overall, the determination of n_{TLS} weakly depends on time in both the experimental measurements where quantum dynamics is at play and in our simulations involving classical exploration of the landscape. However, the physical origin is quite distinct in both situations, and this renders a direct quantitative comparison with experiments delicate.

In the following, we discuss in more detail each step of the construction of the DW library discussing, in particular, in a more detailed way the behavior of the different terms in Eq. (3).

B. Metallic glass model

We simulate a ternary mixture of Lennard-Jones (TLJ) particles in three dimensions. Two particles i and j at positions $\mathbf{r}_i$ and $\mathbf{r}_j$ separated by a distance $r_{ij} = |\mathbf{r}_i - \mathbf{r}_j|$ interact with a Lennard-Jones (LJ) pairwise potential $V(r_{ij})$, given by

$$V(r_{ij}) = 4\varepsilon_{ij}\left[\left(\frac{\sigma_{ij}}{r_{ij}}\right)^{12} - \left(\frac{\sigma_{ij}}{r_{ij}}\right)^{6}\right] + S(r_{ij}), \quad (4)$$

if the particle pair distance $r_{ij}/\sigma_{ij} = x_c$ is within a cutoff distance, $x_c < 2.5$, and have no interaction if their pair distance exceeds that.

To remove any resulting discontinuities from this truncation, we consider the smoothing polynomial,[42]

$$S(r_{ij}) = 4\varepsilon_{ij}\left[C_0 + C_2\left(\frac{r_{ij}}{\sigma_{ij}}\right)^{2} + C_4\left(\frac{r_{ij}}{\sigma_{ij}}\right)^{4}\right]. \quad (5)$$

The choice of coefficients: $C_0 = 10/x_c^6 - 28/x_c^{12}$, $C_2 = 48/x_c^{14} - 15/x_c^8$, and $C_4 = 6/x_c^{10} - 21/x_c^{16}$, ensures the continuity of the potential $V(r_{ij})$ and of its first two derivatives at the cutoff x_c.

We consider three distinct types of particles, A (large), B (small), and C (medium), in a ratio A:B:C = 4:1:1. The unit length is σ_{AA}, and the unit energy is ε_{AA}, noted as σ and ε for simplicity. The interaction parameters are $\varepsilon_{AB} = 1.5\varepsilon$, $\varepsilon_{AC} = 0.9\varepsilon$, $\varepsilon_{BB} = 0.5\varepsilon$, $\varepsilon_{BC} = 0.84\varepsilon$, and $\varepsilon_{CC} = 0.94\varepsilon$ for the energies and $\sigma_{AB} = 0.8\sigma$, $\sigma_{AC} = 1.25\sigma$, $\sigma_{BB} = 0.88\sigma$, $\sigma_{BC} = 1.0\sigma$, and $\sigma_{CC} = 0.75\sigma$ for the ranges. All particles have the same mass m. The unit time is $\tau_{LJ} = \sqrt{m\sigma^2/\varepsilon}$.

This ternary mixture is an extension of the well-known Kob–Andersen (KA)[43] model with a third particle type (C), ensuring resistance against crystallization and increased efficiency for equilibration with the swap Monte Carlo (MC) algorithm, as detailed in Ref. 31 where the model is referred to as KA$_2$. We simulate N particles at number density $\rho = N/L^3 = 1.35$ in a cubic box of linear size L with periodic boundary conditions. This particle density is higher than the commonly investigated value $\rho = 1.2$.[43] Indeed, the pairwise attraction gives rise to a liquid–gas spinodal at low enough temperature, which may intersect the glass transition line,[44] leading to a gas–glass instability.[45] The choice $\rho = 1.35$ ensures the stability of all the studied glasses, as revealed by positive values for the equilibrium pressure of the liquid down to the lowest temperatures investigated, $T = 0.488$. Our model size $L \sim 9.6\sigma$ is large enough to avoid finite-size effects on isolated TLS, but small enough to make it unlikely to observe more than one TLS in a single configuration.

C. Supercooled liquid dynamics and glass preparation

Once the details of the model have been established, one has to estimate the relevant temperatures that govern its glassy dynamics. These are the onset temperature T_o, the mode-coupling temperature T_{mct}, and the laboratory glass transition temperature T_g.

To this aim, standard molecular dynamics has been carried out using the Large-scale Atomic/Molecular Massively Parallel Simulator (LAMMPS) code.[46] A time step of $dt = 5 \times 10^{-3} \tau_{LJ}$ together with a Nosé–Hoover thermostat was used to sample the canonical (NVT) ensemble.

A hybrid swap MC/MD dynamics was also carried out using a modified version of LAMMPS, as detailed in Ref. 47. Based on previous work,[31] we have found that short blocks of ten MD steps with $dt = 5 \times 10^{-3} \tau_{LJ}$ interspersed with blocks of 2100 $(1.75 \times N)$ attempted particle swaps produce the optimal speed-up of the dynamics of this system in the deeply supercooled regime. We recall that both the standard and swap dynamics sample the
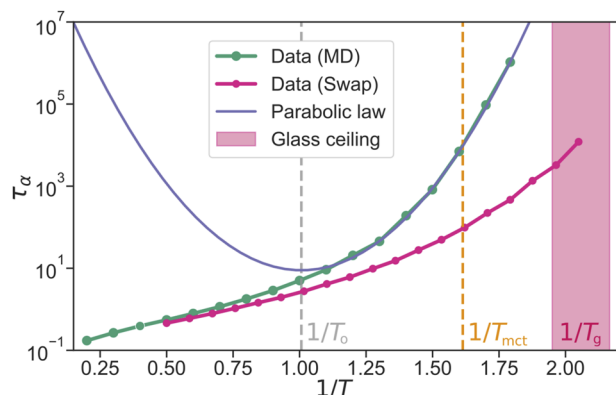
FIG. 1. Angell plot of relaxation time τ_α vs inverse temperature measured in physical molecular dynamics (MD, green) and equilibration particle-swap dynamics (swap, magenta). The onset $T_o \simeq 1.0$ (gray) and mode-coupling crossover $T_{mct} \simeq 0.62$ (orange) temperatures are located with dashed lines. The parabolic fit (purple) is used to extrapolate the relaxation time data at lower temperature. The shaded region between a VFT and parabolic law extrapolation for T_g locates the "glass ceiling."

same equilibrium thermodynamics of the system, provided that proper decorrelation can be achieved within the simulation time window.[29]

In order to monitor structural relaxation during standard and swap MC dynamics, we have estimated the structural relaxation time τ_α from the self-intermediate scattering function $F_s(q = 7.2, t = \tau_\alpha) = 1/e$. The relaxation time τ_α is plotted against inverse temperature in the manner of an Angell plot in Fig. 1.

The onset of glassy dynamics is located at $T_o \sim 1.0$, where the relaxation time data of MD dynamics start to deviate from a log-linear Arrhenius dependence valid at higher temperatures. To obtain T_{mct}, we fit the relaxation times to a power-law behavior, $\tau_\alpha \propto (T - T_{mct})^{-\gamma}$, in a region of moderate supercooling, which results in an empirical estimate of $T_{mct} \sim 0.62$. Finally, the laboratory glass transition temperature T_g is the temperature at which $\tau_\alpha(T_g) = 10^{12}\tau_o$, in microscopic units. Simulations of such long time scales are not tractable, so this temperature is obtained from extrapolations of the available data. Two extrapolations have been used: the Vogel–Fulcher–Tammann law[48] and the parabolic law.[49] These extrapolations define a range for the laboratory glass transition temperature of $T_g \sim 0.46$–0.51, which we refer to as a "glass ceiling," because experiments cannot easily access temperatures lower than T_g. Swap dynamics accelerates the relaxation by up to 8 orders of magnitude at T_g and enables the preparation of deeply supercooled configurations of the TLJ model, equilibrated in the liquid state near the glass ceiling. This allows us to explore for the present model of a metallic glass a broad range of fictive temperatures.

D. Landscape exploration via classical molecular dynamics

To explore the energy landscape, we used an in-house standard MD code in order to have better control over the exploration workflow. The equations of motion were integrated with a smaller time step of $dt = 2.5 \times 10^{-3}\tau_{LJ}$ to ensure a good quality of the structures sampled and to adequately distinguish between distinct IS. Initial velocities are chosen from the Maxwell–Boltzmann distribution at $T_{exp} = 0.4 < T_g$, and temperature is then kept constant by using a Berendsen thermostat.[50] This very low exploration temperature is meant to confine the exploration to the glass metabasin selected by the initial conditions, while still allowing the system to cross enough energy barriers within the metabasin. We have carefully checked that, because standard MD is essentially arrested at those temperatures (Fig. 1), no diffusion is observed. The mean-squared displacement reaches a plateau over a microscopic time and does not grow above it. Hence, the glass metabasin exploration is fully driven by the thermal vibrations of the particles at T_{exp}, and no significant change in the solid structure is detected.

Once every τ_{cg}/dt MD steps, we use the current configuration as the initial state to minimize the energy via a conjugate gradient algorithm to obtain an inherent structure. We repeat this procedure N_{cg} times until a large library of ISs is obtained, reaching a simulation time $\tau_{total} = N_{cg}\tau_{cg}$.

Once a library of ISs has been constructed, we need to select IS pairs as likely candidates to be connected by a path having a double-well potential shape. To this aim, we select pairs of ISs that appear consecutively in the exploration dynamics and record the number of transitions between IS α and IS β in a matrix $T_{\alpha \to \beta}$, where the labeling is ordered by energy (see Fig. 2). If a transition occurs between α and β in both directions at least once ($T_{\alpha \to \beta} \geq 1$ and $T_{\beta \to \alpha} \geq 1$), we consider that the pair (α, β) is a good candidate double-well potential and we attempt to evaluate the MEP between them.

Once a library of candidate transitions is obtained from the minima, the MEP is found using the string method of Ref. 51, which is implemented in LAMMPS as a modification of the nudged-elastic band (NEB) approach.[40] We used $N_{images} = 64$ images of the system to interpolate between the two IS. The images are connected by harmonic springs with a spring constant $\kappa = 0.125\,\varepsilon\sigma^{-2}$. The optimization of the string method was done using the fast inertial relaxation engine (FIRE) minimizer,[52,53] while interpolation of the MEP was carried out with a cubic spline. This should result in an error scaling as $O(N_{images}^{-4})$.[54] The location of the transition state is identified using a climbing image approach.[55] Finally, we check whether the converged MEP contains any intermediate minimum. If not, we preserve it as a "good" double-well potential. Those with intermediate minima can be recurrently refined by splitting into elementary double-well potentials if these intermediate transitions are not already sampled in the dynamics.

The parameters and results of the landscape exploration are summarized in Table I. The data are split between two datasets. Dataset 1 is a coarse sampling with a long minimization period τ_{cg} and a relatively small number of independent glass metabasins N_g at three preparation temperatures: $T_f = 0.509, 0.558, 0.617$. Dataset 2 is a finer and more extensive sampling, with a short minimization period τ_{cg}, a large number of independent glass metabasins N_g, and covering four temperatures, $T_f = 0.488, 0.509, 0.558, 0.617$. The use of two datasets allowed us to validate our choices for the many parameters involved in the construction of a library of double-wells.
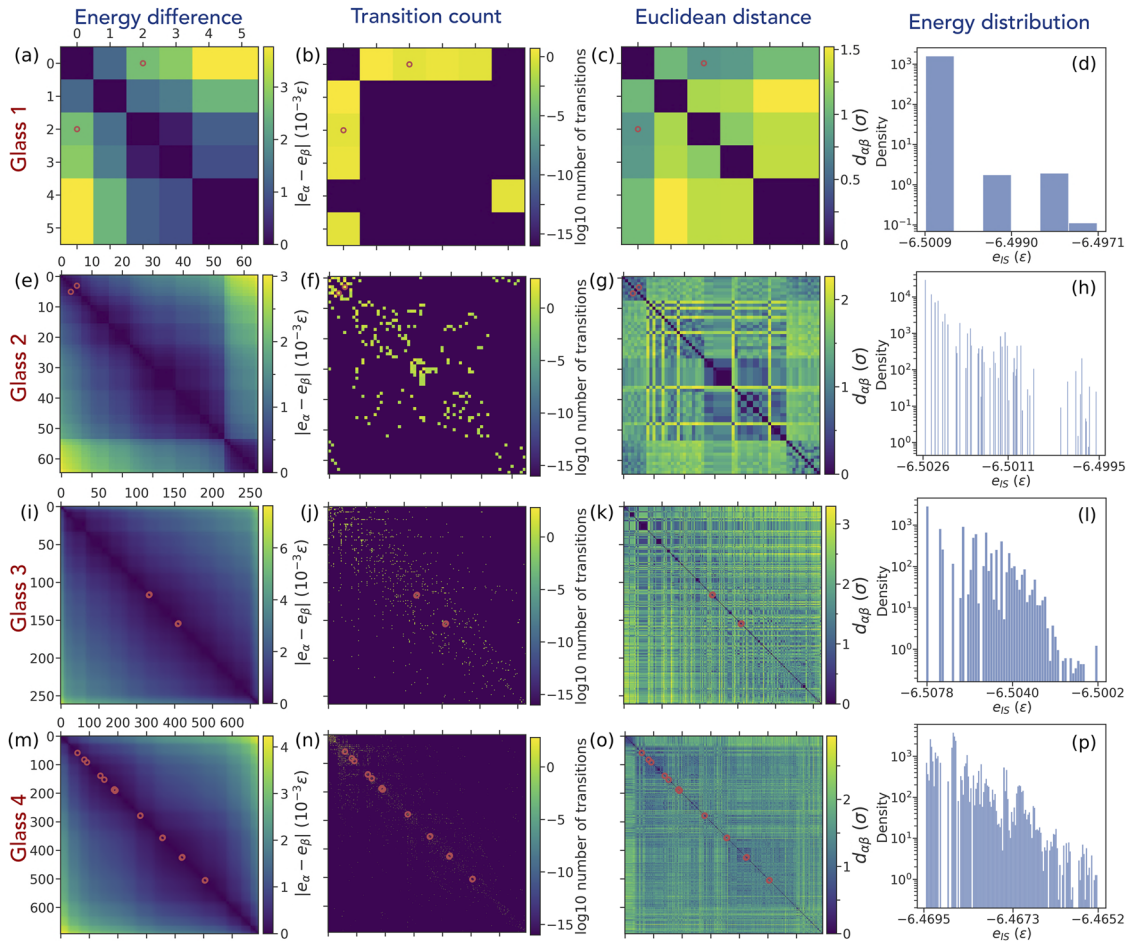
FIG. 2. Heterogeneity of the potential energy landscape of four different glass metabasins labeled in *red* on the left-hand side. Every row corresponds to a glass prepared at $T_f = 0.488$ and sampled at $T_{exp} = 0.4$. In each glass, distinct inherent structures (ISs) are labeled with Greek letters $\alpha = 0, 1, \ldots, n_{IS} - 1$ in order of increasing energy e_α. Each column corresponds to a different observable, labeled at the top in *blue*. The first three columns correspond to matrices where values are evaluated for every pair of minima in a given glass. A consistent color map (viridis) is used for all matrices, with *purple* highlighting a low value and *yellow* highlighting a large one. First column: (a), (e), (i), and (m): matrix of IS energy difference $|e_\alpha - e_\beta|$ in units of $10^{-3}\varepsilon$. Second column: (b), (f), (j), and (n): matrix $T_{\alpha \to \beta}$ counting the number of observed transitions from α to β, shown in a log-scale. Third column: (c), (g), (k), and (o): matrix of Euclidean distance $d_{\alpha\beta}$ in units of σ. Fourth column: (d), (h), (l), and (p): probability density function of IS energies. Red circles indicate the transitions that correspond to tunneling two-level systems.

TABLE I. Summary of the parameters used and the obtained statistics in the landscape exploration of the metallic glass model. Two independent datasets are used. The ratios are evaluated at the end of the exploration protocol $t = \tau_{total}$.

	Dataset 1			Dataset 2			
T_f	0.617	0.558	0.509	0.617	0.558	0.509	0.488
N_g	16	64	256	128	256	512	1 024
τ_{cg}	11	17	43	2	3	18	31
N_{cg}	160 000	40 000	10 000	100 000	100 000	100 000	100 000
τ_{total}	1 760 000	680 000	430 000	200 000	300 000	1 800 000	3 100 000
N_{IS}	36 247	23 287	30 180	70 326	88 112	119 159	117 780
N_{DW}	10 039	8 359	12 117	11 841	20 692	41 342	38 027
N_{TLS}	40	20	41	34	61	137	125
N_{IS}/N_g	2.27×10^3	3.64×10^2	1.18×10^2	5.49×10^2	3.44×10^2	2.33×10^2	1.15×10^2
N_{DW}/N_{IS}	2.77×10^{-1}	3.59×10^{-1}	4.01×10^{-1}	1.48×10^{-1}	2.35×10^{-1}	3.47×10^{-1}	3.23×10^{-1}
N_{TLS}/N_{DW}	3.98×10^{-3}	2.39×10^{-3}	3.38×10^{-3}	2.87×10^{-3}	2.96×10^{-3}	3.31×10^{-3}	3.29×10^{-3}

III. TUNNELING STATES IN THE POTENTIAL ENERGY LANDSCAPE

A. Statistics of potential energy minima

Landscape exploration of large glassy systems is an arduous task as the number of minima is expected to scale exponentially in the number of particles.[37,38] Equilibrium configurations prepared with swap Monte Carlo at a temperature T_f $(T_g < T_f < T_{mct})$ are used to start long MD runs (~10^5 steps) during which the system is quenched to a lower temperature $(T_{exp} < T_f)$.

We can assign to each IS α its energy

$$e_\alpha = \frac{1}{N} \sum_{i<j} V_{ij}(|\mathbf{r}_i^{(\alpha)} - \mathbf{r}_j^{(\alpha)}|) \qquad (6)$$

and compute the Euclidean distance between a pair (α, β) of ISs as

$$d_{\alpha\beta} = \sqrt{\frac{1}{N} \sum_{i=1}^{N} |\mathbf{r}_i^{(\alpha)} - \mathbf{r}_i^{(\beta)}|^2}, \qquad (7)$$

where $\mathbf{r}_i^{(\alpha)}$ is the position of the ith particle in the αth IS.

Figure 2 gives a pictorial overview of the results of the exploration process for four distinct glass metabasins at the lowest $T_f = 0.488$. Each row corresponds to a glass metabasin, ordered from top to bottom by increasing the number of ISs sampled during exploration. From left to right, the following quantities are displayed: the matrices of the energy differences, of transitions, and of Euclidean distances between IS and the probability density function (PDF) of the IS energies e_α observed during exploration. The ISs in the matrices are ordered by increasing energy e_α. The pairs of minima corresponding to TLS are indicated by red circles in all the matrices; they, typically, are found near the diagonal, which means that the two minima forming a TLS are close in energy.

The most striking aspects that emerge from Fig. 2 are (i) the large heterogeneity of the number of ISs (we find between $n_{IS} \sim 6$ and $n_{IS} \sim 600$ ISs in a single metabasin) observed even at this low T_f near the estimated T_g; (ii) the fact that individual ISs are clustered both in energy and in Euclidean distance, as shown, e.g., by the block structure of the $d_{\alpha\beta}$ matrix;[56-58] (iii) the fact that the number of transitions recorded during exploration scales roughly as the number of minima, which is apparent from the sparse and linear scaling nature of non-zero elements of the transition matrix; and (iv) the fact that low energy ISs are sampled repeatedly within the metabasin and the PDF decays with increasing IS energy, as expected from a Boltzmann distribution.

To obtain a more quantitative insight, we first perform exploration runs with $\tau_{cg} = dt$, i.e., minimizing the potential energy at every MD step. The number of distinct ISs per glass is counted, and a distribution of persistence times (τ_p) is inferred from the resulting time series: here, τ_p is the total time during which the energy minimization always ends in the same IS before a new IS is found in the next step. The cumulative distribution function (CDF) of τ_p, for different T_f, is shown in Fig. 3(a). The shape of the CDF indicates that the distribution of τ_p is bimodal, with a first peak around $\tau_p \sim dt$ (i.e., a single MD step) and a second one around $\tau_p \sim 10^2 dt$. A more careful analysis of the IS time series reveals that the peak at short τ_p corresponds to processes during which the system jumps from a low-energy IS to a higher energy IS where it stays for one or two steps,
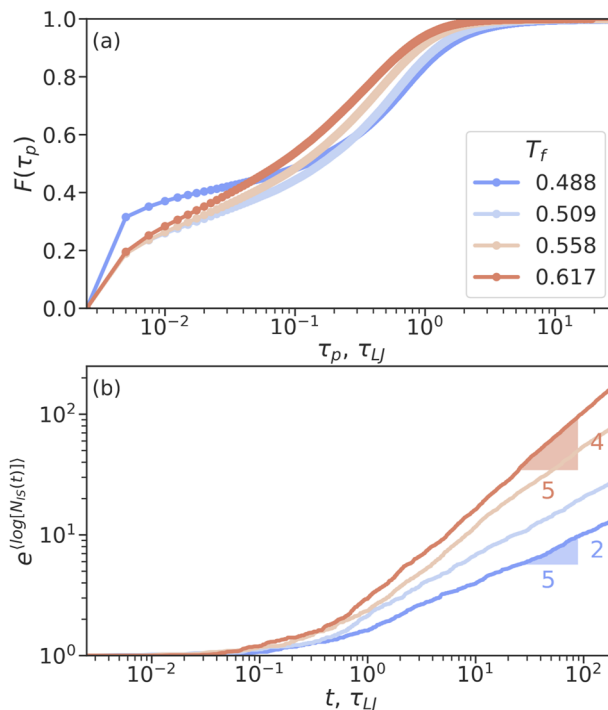
FIG. 3. (a) Cumulative distribution function of the persistence time τ_p between distinct consecutive ISs in the landscape exploration when minimizing every MD step at $T_{exp} = 0.4$. (b) Number of newly found ISs vs time, geometrically averaged over 88 distinct glasses. Colors code for the glass preparation temperature T_f.

before transiting back to the low-energy IS. These processes are associated with strongly asymmetric double-well potentials, which do not give rise to TLSs.

Figure 3(b) shows the logarithm of the number of distinct ISs obtained during exploration of a given glass metabasin, $n_{IS}(t)$, averaged over glasses, as a function of the number of steps for different T_f. We chose to average the logarithm of n_{IS} in order to make sure that the average would not be dominated by rare metabasins with many IS. We, however, found that taking the logarithm of the average, i.e., $\log[N_{IS}(t)/N_g]$, yields similar results.

We find a sub-linear power-law dependence of the number of minima on the exploration time, i.e.,

$$\langle \log(n_{IS}) \rangle \propto \beta \log(t/\tau_0) \approx \log[N_{IS}(t)/N_g], \qquad (8)$$

with an exponent $\beta \in [0.4, 0.8]$ depending on the preparation temperatures considered. As T_f decreases, the typical persistence time increases, and the total number of minima per glass, at a given time t, decreases. This reflects the already well-documented trend that glass metabasins tend to become much simpler in more stable glasses.[56]

The results of Fig. 3(a) suggest that one can make the exploration process more efficient by performing the energy minimization (that is computationally costly) after every τ_{cg}/dt MD steps only, instead of after every step. We have chosen τ_{cg} in our final data production runs for landscape exploration as a compromise between accuracy and efficiency. A low value of τ_{cg} results in a more accurate

count of minima and transitions, with fewer cases where intermediate minima need to be resolved. However, it can be computationally demanding to minimize too frequently as new minima appear in significant numbers only after ~100 – 1000 steps. The values τ_{cg} employed are provided in Table I.

We do not observe any saturation of the total number of IS $N_{IS}(t)$, with growing exploration time t. As a result, we cannot perform an exhaustive search of all the IS within a glass metabasin, as can be expected for a system of mesoscopic size (1200 atoms). Yet, the average number of minima found in each glass basin, N_{IS}/N_g, is strongly depleted with increased glass stability at each fixed t. We can conclude that more stable glasses have fewer ISs, provided that the exploration time of the metabasin exceeds $t \sim \tau_{LJ}$. The time unit τ_{LJ} seems to be close to the characteristic time for moving outside of the basin of a single IS. In the real system at 1 K, one might also expect that only a subset of minima are visited. However, in that case, exploration is dominated by tunneling through barriers and not by crossing them, as in our classical simulations.

B. Identification of double-well potentials

We now want to understand whether our landscape exploration protocol is able to identify all the relevant double well potentials. To this aim, for each DW potential, we measure the first time t at which the corresponding IS pair passes all the filters to be considered a candidate transition: both ISs have been included in the library, and the conditions $T_{\alpha \to \beta} \geq 1$ and $T_{\beta \to \alpha} \geq 1$ are met. We then compute the number of detected DWs and TLSs (defined in Sec. III C) as a function of t, shown in Fig. 4(a) for glasses prepared at the lowest temperature $T_f = 0.488$. Similar results are obtained at all temperatures. We observe that the growth of the number of detected transitions with exploration time is slower than that of the number of IS and is somehow intermediate between a power-law with a small exponent and a logarithmic asymptotic behavior. The growth in the number of TLS qualitatively matches that of the DW.

Assuming logarithmic behavior, a comparison with Eq. (8) gives $N_{DW}(t) \propto \log t \propto \log N_{IS}(t)$, which suggests that we are able to identify the proper elementary excitations of our system, as discussed in Appendix A; see the discussion after Eq. (A2). A faster growth of N_{DW} with N_{IS}, which remains compatible with our data, would suggest that interactions between elementary excitations play a role. This result also implies that even if we are unable to reach a proper saturation of the IS library with exploration time, we are instead able to achieve a much more satisfactory saturation of the DW library. This suggests that the new ISs discovered at large times correspond to combinations of already detected excitations.

We also note that the connectivity of the explored IS as encoded in the ratio N_{DW}/N_{IS} shown in Fig. 4(b) remains of order one and has a mild dependence on the exploration time. Note that this mild time-dependence is still compatible, with N_{DW} being logarithmic in time and N_{IS} being a power-law with a small exponent. We provide the equivalent of Fig. 4 for the polydisperse soft sphere model in Appendix B, Fig. 12.

C. Estimation of quantum tunneling

Two-level systems within our glassy models correspond to tunneling DW potentials with a low quantum splitting. The temperature
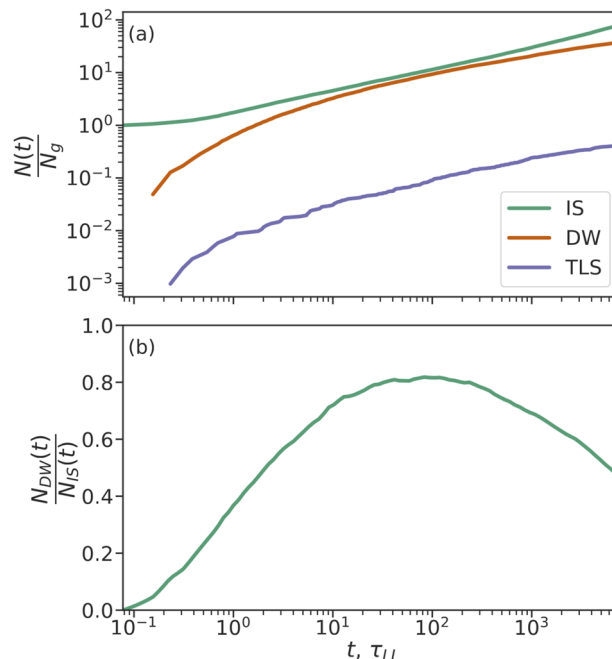
FIG. 4. (a) Number of inherent structures (green), double-wells (orange), and two-level systems (purple) sampled in glasses ($T_f = 0.488$) as a function of exploration time. The number of ISs grows as a power-law, while the growth of DWs is slower at long times. TLSs follow the same time evolution as DW. (b) Ratio of the number of DWs to that of ISs as a function of exploration time. The two panels share the horizontal axis.

scale below which quantum effects are important is $T_Q \sim 1$ K in experiments and can be obtained from comparing the interparticle distance with the thermal wavelength, leading to

$$T_Q = \frac{2\pi\hbar^2}{m\sigma^2 k_B}. \tag{9}$$

The MEP obtained via a converged optimization of the string method, with no intermediates, results in a 1D potential energy profile, as schematized in Fig. 5. By convention, the lowest energy minimum is taken to be the one on the left. From this simplified 1D potential, several quantities can be defined: the forward barrier, V_a, is the energy difference between the transition state and the lowest energy minimum; the asymmetry, ΔV, is the difference in energy between the two minima, and the barrier height can be obtained from these two quantities: $V_b = V_a - \frac{1}{2}\Delta V$.

As a first approximation, we reduce the tunneling problem to the effective one-dimensional potential of the MEP. Considering a normalized reaction coordinate $\xi \in [0, 1]$, which corresponds to the fraction of the Euclidean distance d along the minimum energy path, we can write the resulting Schrödinger equation as

$$-\frac{\hbar^2}{2md^2\varepsilon}\partial_\xi^2\psi(\xi) + V(\xi)\psi(\xi) = \varepsilon\psi(\xi). \tag{10}$$

An interpolated MEP obtained from the NEB calculation is discretized by $d\xi = d/N_\xi$, where $N_\xi = 2000$, using a cubic spline. The
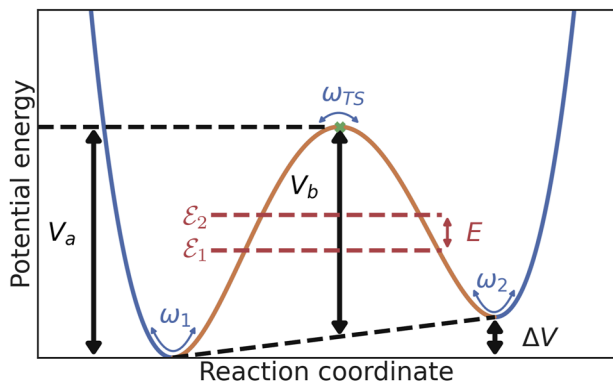
FIG. 5. Schematic representation of a double-well potential illustrating the approximate MEP obtained numerically (orange) and its extrapolation beyond the two minima (blue), along with the forward barrier V_a, asymmetry ΔV, barrier height $V_b = V_a - \Delta V/2$ (black arrows), and the curvature of the potential-energy surface at the lowest minimum ω_1, highest minimum ω_2, and transition state ω_{TS} (blue curved arrows). The quantum splitting E is the difference between the first two quantum energy levels ε_1 and ε_2 (red dashed lines).

Laplacian is evaluated with a five-point finite difference stencil. We use $\hbar = 1$ to evaluate the quantum properties of the DW. This leads to a dimensionless effective mass parameter $\tilde{m}$, which controls the "quantumness" of the problem, as first introduced by Vineyard,[59]

$$\tilde{m} = m \frac{\varepsilon \sigma^2}{\hbar^2}. \tag{11}$$

The MEP and the effective mass $\tilde{m}$ define a 1D potential for the DW excitation. We assume that the tunneling problem can be treated in a 1D approximation when the relevant classical path, the MEP, is nearly independent of the others.[18] We have calculated the eigenvalues and eigenvectors of the Hessian along the MEP to check that orthogonally to the MEP, the dynamics is harmonic and independent of the reaction coordinate. The results are summarized in Appendix C, and in Fig. 13.

The $\tilde{m}$ parameter depends on the choice of units. Nevertheless, it can be tuned over a wide range of values (10^2–10^5) without changing the qualitative behavior of the quantum splitting distribution obtained from our simulations.[21] In this case, for the two sets of units detailed in Sec. IV B, namely, argon (Ar) and nickel–phosphorous (NiP), the value of $\tilde{m}$ is 1200 and 5250, respectively. The corresponding values of $k_B T_Q$ are 0.005ε (for Ar) and 0.0012ε (for NiP).

The five smallest eigenvalues $\varepsilon_1, \ldots, \varepsilon_5$ are then evaluated using ARPACK.[60] The splitting is given by the first two energy levels, $E = \varepsilon_2 - \varepsilon_1$. We consider as tunneling TLS all the filtered and tunneling DWs that have a splitting $E < T_Q$. Following our notations, their total number is $N_{DW}(T_Q)$.

We can also attempt to map the DW profile into an actual two-level system. In the standard TLS model, the Hamiltonian of a single tunneling state takes the form

$$H = \frac{1}{2} \begin{pmatrix} \Delta & \Delta_0 \\ \Delta_0 & -\Delta \end{pmatrix} \tag{12}$$

in the localized representation. The diagonal splitting of the TLS can be estimated by

$$\Delta = \Delta V + \hbar \frac{\omega_2 - \omega_1}{2}, \tag{13}$$

where ω_1 and ω_2 are the characteristic frequencies of the two minima of the double-well potential; see Fig. 5. The decay rate of the TLS can be evaluated in the Wentzel–Kramers–Brillouin (WKB) approximation as

$$\Gamma = \frac{1}{m} \left[\int_0^a \frac{dx}{p(x)} \right]^{-1} \exp \left[-\frac{2}{\hbar} \int_a^b |p(x)| dx \right], \tag{14}$$
$$p(x) = \sqrt{2m(\varepsilon_2 - V(x))}.$$

The tunneling matrix element Δ_0 can be obtained from the effective one-dimensional potential via the WKB approximation as

$$\Delta_0 \approx \bar{\varepsilon} \exp \left[-\frac{1}{\hbar} \int_a^b |p(x)| dx \right], \quad \bar{\varepsilon} = \frac{\varepsilon_1 + \varepsilon_2}{2}. \tag{15}$$

The integration limits a and b correspond to values of the effective reaction coordinate x where a certain energy level crosses the double-well potential curve at either side of the barrier. This level is ε_2 for the calculation of Γ and $\bar{\varepsilon}$ for Δ_0.

As such, the quantities Δ and Δ_0 are expected to approximately obey the relationship $E \approx \sqrt{\Delta^2 + \Delta_0^2}$. The quantum splitting E is plotted against $\sqrt{\Delta^2 + \Delta_0^2}$ in Fig. 6(a), showing the expected correlation at all temperatures. Small deviations from $E \approx \sqrt{\Delta^2 + \Delta_0^2}$ are observed at low splittings E. These deviations could appear due to the breakdown in the various approximations that are made to calculate E, Δ, and Δ_0. The magnitude of the deviations becomes important as $E \sim 1/N$, suggesting that finite-size effects could influence the absolute magnitude of very low splittings.

Figure 6(b) shows the cumulative probability distribution function $F(\Delta_0)$ of the tunneling matrix element Δ_0. The TLS model predicts a flat PDF for $\log \Delta_0$, which corresponds to $F(\Delta_0) \sim \log \Delta_0$ at small Δ_0. Our data instead suggest that $F(\Delta_0) \sim \Delta_0^\varphi$ with a very small exponent $\varphi \approx 0.1$, corresponding to a PDF $p(\Delta_0) \sim \Delta_0^{\varphi-1}$. Such behavior was discussed in more detail elsewhere.[2,61]

The decay rate Γ is also expected to approximately obey $\Gamma \propto \Delta_0^2 E$ due to Landau–Zener tunneling,[62] which is seen in the inset of Fig. 6(b). Finally, the CDFs of Δ and E are shown in Figs. 6(c) and 6(d), respectively. Below T_Q, both the CDFs of Δ and E are linear, as expected in the TLS model, and change very little with T_f.

The ratio of tunneling TLS to generic double-wells, $N_{DW}(T_Q)/N_{DW}$, seems to be roughly constant ~0.3% at all temperatures. Because the function $N_{DW}(E)/N_{DW}$ converges to a stable finite limit when $N_{DW} \to \infty$, the ratio $N_{DW}(T_Q)/N_{DW}$ is also stable in both datasets presented in Table I, indicating that it is not particularly sensitive to the details of landscape exploration.
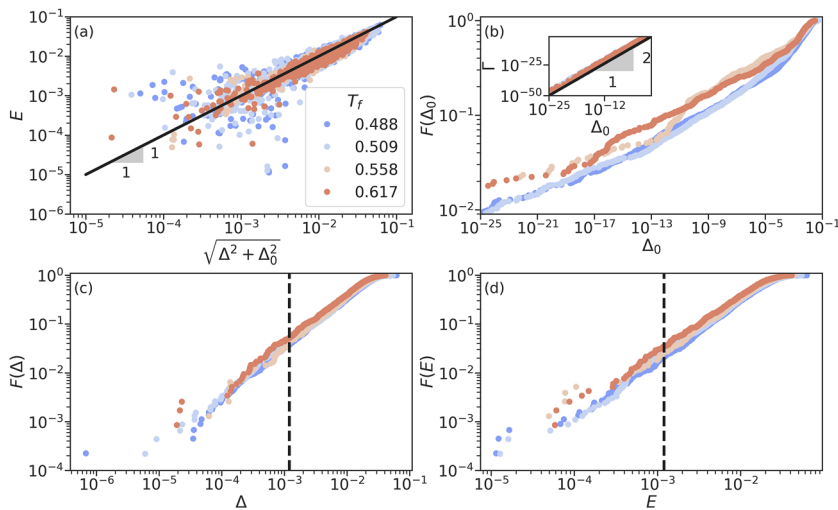
FIG. 6. (a) Scatter plot of the quantum splitting E vs $\sqrt{\Delta^2 + \Delta_0^2}$. Colors code for different preparation temperatures T_f. (b) Cumulative distribution function of the tunneling matrix element Δ_0. Inset: decay rate Γ vs Δ_0 following a $\Gamma \propto \Delta_0^2$ scaling (line). Cumulative distribution functions of (c) the diagonal splitting Δ and (d) the quantum splitting E. Dashed lines indicate $T_Q = 0.0012$. The linear behavior in (c) and (d) below T_Q directly validates the hypothesis of the TLS model. Data in all panels were calculated using $\tilde{m} = 5250$, corresponding to NiP units.

IV. MICROSCOPIC PROPERTIES OF TWO-LEVEL SYSTEMS

A. Statistical properties of two-level systems

The data from the extensive exploration of the energy landscape are summarized in Fig. 7, which presents the statistics of different observables of tunneling DW potentials in relation to their estimated quantum splitting E and the preparation temperature T_f of the glass. The DW asymmetry, ΔV, is shown in Fig. 7(a) where one can note a threshold value $\Delta V \sim 10^{-2}$, below which the distribution of quantum splittings becomes much broader. Asymmetry between energy minima seems to be on average higher for higher preparation temperature T_f.

The statistics of the energy barrier, V_b, vs E are shown in Fig. 7(b). Our dataset probes a range of two orders of magnitude in barrier heights between sampled tunneling DW. In general, DWs with a low splitting E have a relatively high barrier V_b. DWs sampled

in lower T_f glasses typically have a higher barrier than those found in glasses prepared at high T_f.

The statistics of the tunneling decay rate Γ ($\propto \Delta_0^2 \times E$) are shown in Fig. 7(c). The distribution of tunneling decay rates Γ becomes narrower as the tunnel splitting E decreases. On average, the decay rate Γ decreases with the quantum splitting E. Roughly one third of the sampled tunneling DW decay in more than 1 h.

Our numerical study provides information on the microscopic properties of the transition sampled. From a structural point of view, the degree of localization can be evaluated from the atomic displacement $d_{\alpha\beta}^i = |\mathbf{r}_i^{(\alpha)} - \mathbf{r}_i^{(\beta)}|$ of atom i between the two IS α and β by calculating the participation ratio (PR),

$$PR = \frac{\left[\sum_i (d_{\alpha\beta}^i)^2\right]^2}{\sum_i (d_{\alpha\beta}^i)^4}, \tag{16}$$
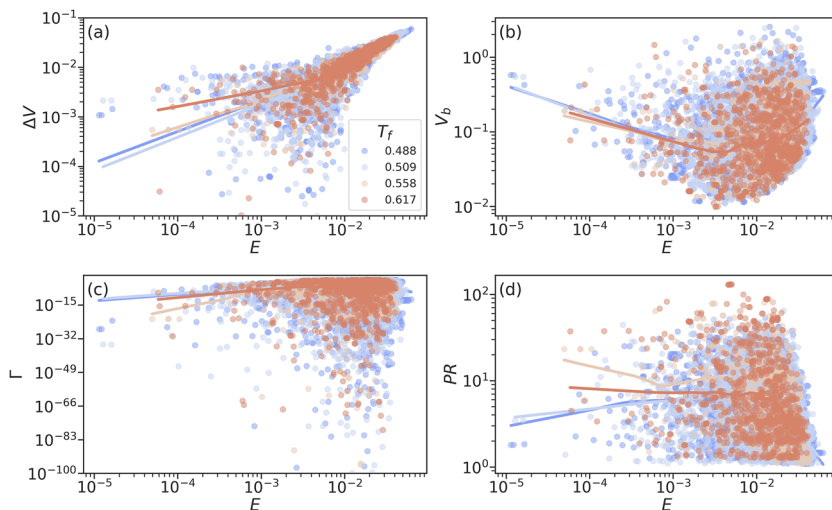
FIG. 7. Statistics of tunneling double-well potentials vs the estimated quantum splitting E: (a) asymmetry ΔV, (b) barrier height V_b, (c) tunneling decay rate Γ, and (d) participation ratio PR. All values were calculated with a reduced mass $\tilde{m} = 5250$, corresponding to NiP units. Colors code for different preparation temperatures T_f. Solid lines correspond to average values at a given E obtained via locally weighted regression.
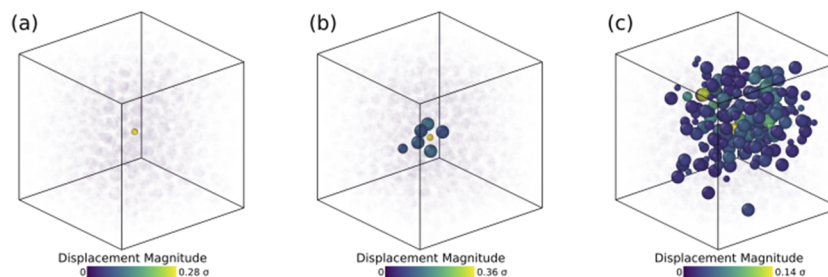
FIG. 8. Visualization of atomic displacements between the two minima forming a double-well (DW) potential with low quantum splitting. Only the particles that displace the most are shown, and the rest are made transparent and faded in the background for clarity. (a) A localized two-level system in which a single particle moves in an almost frozen structure, $PR \sim 1$. (b) A typical two-level system, with $PR \sim 7$. (c) A delocalized two-level system with $PR \sim 83$; these cases are rare and mostly occur in less stable glasses $T_f = 0.617$.

defined such that $1 \leq PR \leq N$. The participation ratio indicates the number of atoms involved in a transition.

The statistics of PR vs E are shown in Fig. 7(d). Most of the displacements observed in our database are localized, and they have an average participation ratio $PR \sim 8$. Even the most delocalized DWs that pass the filtering procedure do not have a PR much larger than 100. We see from Fig. 7(d) that, on average, the PR decreases with decreasing T_f. This can be rationalized in terms of displacements that tend to be more local in more stable glasses.

However, examples of delocalized DWs ($PR \sim 100$) with a low E do exist, but they are found only in glasses prepared at high $T_f \simeq T_{mct}$. Such delocalized excitations correspond to very small individual displacements and have a small barrier. This is a similar pattern to what was also observed in the atomic tunneling of complex crystalline defects, such as kinks in metallic Cu.[63]

We have also looked at the scatter plot of Euclidean distances vs the quantum splitting, which is shown in Fig. 14 in Appendix D. The patterns of real-space atomic displacements between the configurations of the two ISs forming a DW potential are illustrated in Fig. 8. Atoms are shown with a radius proportional to their interaction range σ and colored by $d_{\alpha\beta}^i$, the magnitude of their displacement between the two minima. In order to ease visualization, only the particles that displace the most are shown, with the rest faded into the background for clarity. For clarity, only the first particles up to PR, to the nearest integer, are highlighted. In general, displacements in our database of DWs are highly localized and involve only several atoms. We nevertheless can distinguish three classes of TLSs, similar to a recent study on amorphous Si.[64] The most localized DW potentials have a $PR \sim 1$, such as the one shown in Fig. 8(a). These would correspond to defect hopping within the material. A more typical TLS is shown in Fig. 8(b); it has a $PR \sim 7$. It is still one atom that moves significantly, but this triggers the rearrangement of nearest neighbors as well. Although very rare, we also do find delocalized excitations, see Fig. 8(c), where nearly 10% of the particles move a relatively small distance throughout the whole structure. These tend to occur in less stable, higher $T_f \simeq T_{mct} \simeq 0.62$ glasses.

## B. Depletion of tunneling two-level systems with increasing glass stability

The standard TLS model predicts a plateau $n(E)/E \to n_0$ as $E \to 0$, where $n(E)$ is the cumulative distribution of quantum splittings. The results obtained from our energy landscape exploration of the ternary LJ model are shown in Fig. 9(a). In agreement with the tunneling model, we observe a plateau for $E < T_Q$ (vertical dashed) at all T_f and a peak at $E \sim 5 \times 10^{-2}$. In addition to the low-E plateau behavior observed at each temperature, we identify a clear depletion of $n(E)/E$ as T_f decreases. This agrees with the previous computational estimation of the TLS density as a function of glass stability in polydisperse soft-spheres (PSSs).[21]

In order to compare the TLJ data with the PSS model, we have plotted $n_0/\tilde{m}$ vs the stability of the glass, as encoded in the relaxation time ratio $\log(\tau_\alpha(T_f)/\tau_o)$, in Fig. 9(b). In this representation, glass stability increases from left to right. The relaxation time $\tau_\alpha(T_f)$ is either directly measured or estimated by extrapolating the data to lower temperature using a parabolic law, which was shown to perform well such extrapolation.[65] The n_0 values for PSS are from Ref. 21, while we have refined our τ_α-extrapolation using the latest data obtained via long MD simulations of PSS.[66] The range of glass stabilities explored in the ternary model is roughly two orders of magnitude smaller than in PSS. This is due to the particle-swap algorithm thermalizing more efficiently continuously polydisperse mixtures compared to ternary mixtures. To make a meaningful comparison of the defects in both models, we have estimated the TLS density n_0 after a fixed exploration time of $t = 10^3 \tau_{LJ}$. This is the longest exploration time that can be probed from our simulations, in both models, at all T_f. This restriction has reduced the range of n_0 values showed previously for the PSS model.[21] Nevertheless, at this fixed exploration time, the two models show a similar depletion of two-level systems, with the TLJ model showing a slightly steeper depletion. As evidenced from Table I, this depletion of tunneling defects seems to be driven by a reduction in the number of ISs available in a glass metabasin as T_f decreases. The curves are shown for different values of $\tilde{m}$ to probe quasi-universality by emulating different material properties within the same model. This confirms that the precise value of $\tilde{m}$ does not affect our main conclusion.

The choices of $\tilde{m}$ prompt a short discussion on the units. Two sets of physical units have been investigated in order to make a connection to experimental observations. The first one corresponds to physical units that mimic pairwise interactions between argon (Ar) atoms[18] and has the following parameters: $\sigma = 3.405 \times 10^{-10}$ m, $\varepsilon/k_B = 125.2$ K, and a mass of $m = 6.634 \times 10^{-26}$ kg. The unit of time is $\tau_{LJ} = 2.1$ ps. In these units, the numerically estimated glass
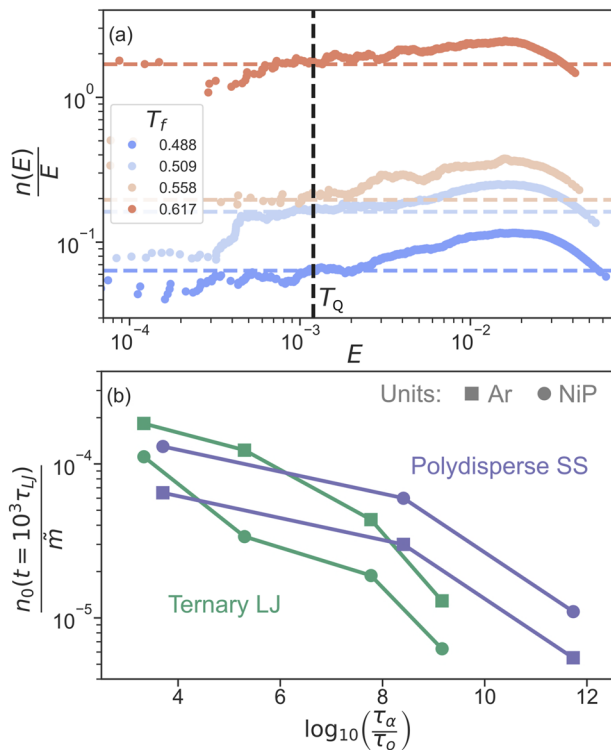
FIG. 9. (a) Cumulative distribution of the quantum splitting E for all tunneling double-well potentials as a function of glass stability T_f ($\tilde{m} = 5250$). Plateau values indicate n_0. (b) Density of two-level systems n_0 in ternary Lennard-Jones (TLJ) and polydisperse soft-sphere (PSS) glasses as a function of stability, as encoded in $\tau_\alpha(T_f)/\tau_o$. Data for two sets of units: NiP (circle, $\tilde{m} = 5250$) and Ar (square, $\tilde{m} = 1200$). PSS data from Ref. 21. To compare the models, we have fixed the exploration time $t = 10^3 \tau_{LJ}$ to estimate n_0.

transition temperature is $T_g \approx 59$ K, $T_Q \approx 0.658$ K, and $\tilde{m} \approx 1200$. For the preparation temperatures $T_f = 0.488, 0.509, 0.558$, and 0.617, one gets $n_0^{sim} \sim 0.04, 0.09, 0.14$, and $0.674\varepsilon^{-1}\sigma^{-3}$, which corresponds to $n_0^{exp} \sim 4.05 \times 10^{47}, 1.19 \times 10^{48}, 2.61 \times 10^{48}$, and 8.95×10^{48} J^{-1} m^{-3}.

The second set of units, used to mimic the average pairwise interactions in a NiP glass,[19,67] consists of the following parameters: $\sigma = 2.21 \times 10^{-10}$ m, $\varepsilon/k_B = 934$ K, and an average mass per particle of $m = 9.266 \times 10^{-26}$ kg. The unit of time is $\tau_{LJ} = 2.5$ ps. In these units, the glass transition temperature is $T_g \approx 438$ K, $T_Q \approx 1.118$ K, and $\tilde{m} \approx 5250$. The defect density is $n_0^{sim} \sim 0.08, 0.19, 0.23$, and $1.84\varepsilon^{-1}\sigma^{-3}$, which corresponds to $n_0^{exp} \sim 4.24 \times 10^{47}, 1.11 \times 10^{48}, 1.53 \times 10^{48}$, and 1.17×10^{49} J^{-1} m^{-3}.

We find a modest variation in the absolute value of the tunneling defect density with $\tilde{m}$. The difference between the defect density of the two models (PSS and TLJ) at the same glass stability is similar in magnitude to the difference between the defect density calculated for different values of $\tilde{m}$, and the data are insufficient to establish any clearer pattern.

A reduction of the number of defects could be expected in the TLJ model due to the change from a polydisperse system in which every particle is different, to one with only three types of indistinguishable particles (A, B, and C). An additional influence could come from the attractive interactions, absent in the PSS model, which have been recently suggested to have an important effect on the elastic properties of glassy solids. In particular, a reduction of the density of quasi-localized modes (QLMs) was reported as the attractive part or "stickiness" of the pair-potential increases.[68] The decrease in QLM density can be up to an order of magnitude and was compared to the reduction in defects observed during thermal annealing. We defer the discussion of the behavior of QLM in these models and their potential relationship to n_0 to Sec. IV C.

C. Comparison to quasi-localized harmonic modes

To begin evaluating the vibrational modes of the TLJ glass configurations, we first estimate their elastic moduli at different T_f from athermal quasistatic deformation simulations. With an initial IS obtained through energy minimization from an equilibrium configuration, a suitable cycle of small deformations is applied, each deformation being followed by an energy minimization, until a stress–strain curve is obtained. The shear modulus G is obtained from athermal quasi-static shear simulations (AQSs) under Lees–Edwards boundary conditions, while the bulk modulus K is obtained from quasistatic deformation with periodic boundary conditions and a hydrostatic strain. The elastic moduli are obtained from the elastic regimes of the corresponding stress–strain curves,

$$G = \frac{\sigma_{xy}}{\gamma_{xy}}, \qquad K = -V\frac{\Delta p}{\Delta V}. \qquad (17)$$

Once the moduli have been determined, we calculate the transverse $c_t = \sqrt{G/(m\rho)}$ and longitudinal $c_l = \sqrt{(K + \frac{4G}{3})/(m\rho)}$ sound velocities, and from them, we calculate the frequency ω_t of the first phonon,

$$\omega_t = \frac{2\pi}{L}c_t, \qquad (18)$$

and the Debye frequency,

$$\omega_D = \left(\frac{18\pi^2\rho}{2c_t^{-3} + c_l^{-3}}\right)^{\frac{1}{3}}. \qquad (19)$$

We have calculated and diagonalized the dynamical matrix to obtain the vibrational modes and their frequencies. This was done for the ensemble of structures in Table I, as well as for larger 12 000-atom TLJ configurations at $T_f = 0.509, 0.558$, and 0.617, using ensembles of 1000 configurations at each T_f. Non-phononic vibrational modes can be seen below the first phonon peak at ω_t when the model size is small enough to avoid significant hybridization with phonons. It is typically assumed that the density of states $D(\omega)$ scales as ω^4 in the low-frequency limit.[70]

In Fig. 10(a), we show the integrated density of states $I(\omega)$, scaled by the expected ω^5 for the larger 12 000-atom models at each T_f. Provided that $D(\omega) \propto A_4\omega^4$, we would expect a plateau in $I(\omega)/\omega^5$ just below ω_t. We find this to be the case; however, the plateau (dashed) persists only over a limited range of frequency, below which the scaling seems to change, in agreement with recent results on the behavior of very-low frequency modes in the standard
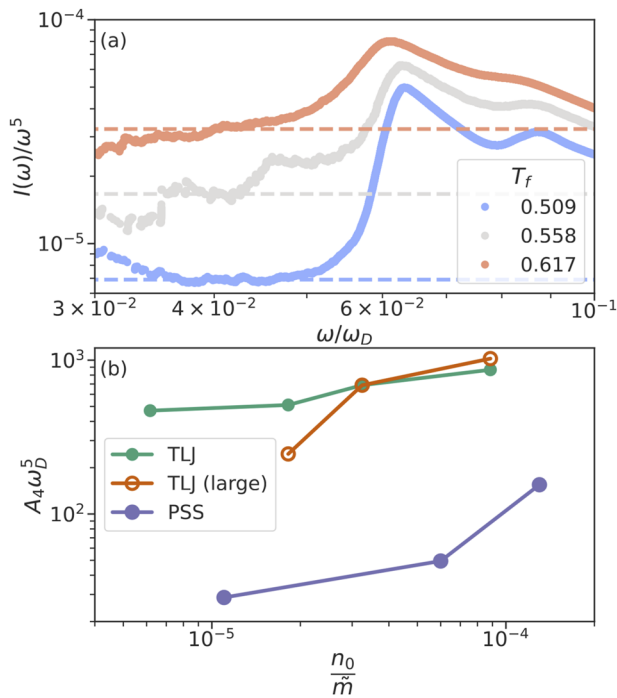
FIG. 10. (a) Integrated density of states, $I(\omega)/\omega^5$, in large $N = 12\,000$ ternary Lennard-Jones (TLJ) glasses prepared at different T_f. Dashed lines represent the $A_4/5$ fits of $I(\omega)/\omega^5$ just below ω_t. (b) A_4 vs n_0 for $N = 1200$ (green) and larger $N = 12\,000$ (orange) TLJ glasses (orange circles) and the polydisperse soft sphere (PSS) configurations from Ref. 21 (purple). The A_4 and ω_D values for the PSS model are from Ref. 69.

KA model.[71] The low-frequency behavior of $D(\omega)$ is currently under intense scrutiny, and this discussion would require much more statistics than we currently possess. Our goal is simpler as we only wish to understand whether the evolution of localized harmonic modes in $D(\omega)$ and of TLS are strongly correlated.

Moving on to the quantitative relationship between QLM and TLS, we report in Fig. 10(b) the adimensional quantity $A_4\omega_D^5$ vs the density of TLS obtained with NiP units. Again, the TLS density n_0 is compared after a fixed exploration time of $10^3\tau_{LJ}$ for both models. Since both quantities decrease with decreasing T_f, they necessarily appear correlated in such a representation, but this of course does not imply any causal relationship.[72] In particular, our data seem to preclude a direct proportionality between the two quantities of the kind predicted in Ref. 33. This is especially true for the more realistic metallic glass model. Interestingly, while the density of TLS of the two models is very similar for glasses of equivalent stability, we find instead an increased density of QLM in the TLJ model. These observations suggest that generic QLMs are poor predictors of TLS even though both families of localized excitations are similarly sensitive to the stability of the glass.

V. CONCLUSIONS

Our analysis confirms that TLSs are depleted with the increasing glass stability in a second, more realistic, and physically distinct glass-forming model.[21] The number of two-level systems converges relatively quickly at ~0.3% of the number of the double-well potentials identified during the classical exploration of the potential energy landscape. As the glass preparation temperature T_f decreases, we find a slowly increasing ratio of the number of double wells over that of minima, which reflects a locally more connected energy landscape. The significant depletion of two-level systems with glass stability is in the end driven by the drastic reduction in the number of minima in a typical glass metabasin as T_f decreases. The number of minima as a function of exploration time increases slowly as a sublinear power-law for all temperatures considered, with an exponent that decreases with decreasing T_f. This means that while the depletion of two-level systems remains robust, an exhaustive counting of both minima and defects remains elusive, even when exploration is strongly confined to a well-defined metabasin.

The exploration of low energy glass metabasins reveals a significant degree of heterogeneity. In particular, we observe very large fluctuations, of several orders of magnitude, in the number of minima present in independent glass basins, even as $T_f \approx T_g$. An analysis of the metabasins from the perspective of connected pairs of ISs shows a hierarchical structure of the energy landscape, as previously observed in Refs. 56–58. The observation of these extremely strong sample-to-sample fluctuations in glass samples deserves further investigation.[73,74]

Comparing the continuously polydisperse soft-sphere system to a more realistic ternary model, such as TLJ, some important differences emerge as well. The absolute number of two-level systems, as estimated from the n_0 values for the TLJ model, are a bit closer to those obtained in real experiments, but remain larger by roughly an order of magnitude. While in the polydisperse model every particle is different, the ternary model contains particles of different types that are indistinguishable, which should decrease the possible number of defects, hence that of minima. From this point of view, glassy materials of increased chemical complexity should naturally exhibit more defects, while monodisperse or elemental counterparts of similar kinetic stability are likely to have fewer low-energy excitations. We observe only a modest effect though, which seems consistent with the experimentally observed quasi-universality of TLS density.

Another factor for the reduced density of two-level systems is the presence of attractive interactions and their influence on barrier heights. Control over the strength of attractive interactions may help modulate the properties of glassy materials through the reduction of low-energy excitations, but trade-offs might come in to play with other types of defects, such as quasi-localized modes. Other interaction potentials could also be studied in order to better understand the role played by many-body interactions, anisotropy, and dimensionality.

When attempting to perform a quantitative comparison of the number of TLS observed in experiments and in computer simulations, one should keep in mind that in experiments, landscape exploration is driven by quantum tunneling at ~1 K, which leads to a characteristic $\log(t)$ dependence of the TLS density, while in our computer study, the landscape exploration is driven by classical thermal fluctuations at temperatures much higher than 1 K, leading to a power-law growth of the number of minima with time. A direct comparison is then probably hindered by this important difference.

We have also explored the nature of the relationship between quasi-localized modes and two-level systems. We find the density of two-level systems to be correlated with that of quasi-localized modes, but we do not find them to be proportional or related by any causal link. At very low frequency, modes may no longer obey an ω^4 scaling although large uncertainties are present in our data. Interestingly, while the two models have a similar density of TLS, the density of QLM seems to increase for the TLJ model. This observation suggests that there is a diversity of defects present in glasses at low temperatures, which still evade an exhaustive classification.

As perspectives for further numerical studies, we would like to delineate three important research directions. First, to make our main conclusion linking glass stability to the depletion of the density n_0 of TLS even stronger, some of the approximations used to estimate n_0 should be removed from simulations. The most ambitious task would be to explore the landscape and obtain the quantum splitting for candidate TLS from a fully quantum-mechanical calculation using path-integral methods.[75,76] A second task would be to improve the computational tools used in this work to significantly increase the library of TLS through the use of techniques in enhanced sampling and machine learning. Third, the discovery that glass metabasins contain such a large number of minima organized in a way that depends on glass stability, although hinted by previous work, requires a dedicated study to better quantify this evolution and understand how it impacts the physical properties of glassy and viscous liquid states.

ACKNOWLEDGMENTS

AUTHOR DECLARATIONS

Conflict of Interest

The authors have no conflicts to disclose.

Author Contributions

Felix C. Mocanu: Conceptualization (equal); Data curation (lead); Formal analysis (equal); Investigation (lead); Methodology (equal); Resources (equal); Software (equal); Validation (lead); Visualization (equal); Writing – original draft (lead); Writing – review & editing (lead). **Ludovic Berthier**: Conceptualization (equal); Formal analysis (equal); Investigation (equal); Methodology (lead); Supervision (equal); Validation (equal); Visualization (equal); Writing – review & editing (equal). **Simone Ciarella**: Formal analysis (supporting); Software (supporting); Validation (supporting); Writing – review & editing (supporting). **Dmytro Khomenko**: Data curation (supporting); Validation (equal); Visualization (supporting); Writing – original draft (supporting); Writing – review & editing (supporting). **David R. Reichman**: Conceptualization (supporting); Formal analysis (supporting); Validation (supporting); Writing – review & editing (supporting). **Camille Scalliet**: Conceptualization (supporting); Methodology (equal); Software (lead); Validation (equal); Visualization (equal); Writing – review & editing (equal). **Francesco Zamponi**: Conceptualization (equal); Formal analysis (equal); Funding acquisition (lead); Investigation (lead); Project administration (lead); Resources (equal); Supervision (equal); Validation (equal); Writing – original draft (equal); Writing – review & editing (equal).

DATA AVAILABILITY

The data that support the findings of this study such as the statistics of sampled double-well potentials and equilibrium configurations of the ternary Lennard-Jones model are openly available at http://doi.org/10.5281/zenodo.7117711.

APPENDIX A: LARGE-SCALE BEHAVIOR OF N_{DW}/N_{IS}

We discuss here the behavior of N_{DW}/N_{IS} in the limit of a large number of samples and particles. Let us consider, as an example, a large system having K independent localized excitations (i.e., DW potentials associated with the displacement of a few atoms). Note that within the TLS model, K should be proportional to the number of atoms N, provided that N is large enough. Each DW can be represented by a one-dimensional local reaction coordinate x_i, with an associated potential taken, for the sake of illustration, to be of the form

$$v_i(x_i) = \frac{1}{4!}x_i^4 + \frac{1}{2}\kappa_i x_i^2 - h_i x_i. \tag{A1}$$

If $\kappa_i^3 + 9h_i^2/8 < 0$, this potential has two local minima, leading to a DW with energy splitting $\Delta V_i(\kappa_i, h_i)$. Let us introduce a spin variable $\sigma_i = 0, 1$ if x_i is in the absolute, respectively, local, minimum of $v_i(x_i)$. If the excitations are diluted and thus do not interact, the total energy of the system can be written as

$$V(\{x_i\}) = \sum_{i=1}^{K} v_i(x_i) \quad \Rightarrow \quad E_{IS}(\{\sigma_i\}) = \sum_{i=1}^{K} \Delta V_i \sigma_i. \tag{A2}$$

Such a system has $N_{IS} = 2^K$ local minima, corresponding to all possible combinations of the σ_i, with energy $E_{IS}(\{\sigma_i\})$. On the other hand, we have $N_{DW} = K$, with each IS being connected to K others: in fact, the MEP associated with a composite excitation of the form $(\sigma_i = 0, \sigma_j = 0) \rightarrow (\sigma_i = 1, \sigma_j = 1)$ would be decomposed into elementary events, e.g., $(\sigma_i = 0, \sigma_j = 0) \rightarrow (\sigma_i = 0, \sigma_j = 1) \rightarrow (\sigma_i = 1, \sigma_j = 1)$, leading to the appearance of an intermediate local minimum in $(\sigma_i = 0, \sigma_j = 1)$ in the MEP. This very simple argument thus suggests a relationship of the kind $N_{DW} \approx \log N_{IS}$.

In summary, for $K \propto N$ independent excitations in each glass and for N_g glasses, we would have in total $N_{IS} \sim N_g \exp(K) \sim N_g \exp(N)$, $N_{DW} \sim N_g K \sim N_g N$, and $N_{DW}/(NN_g)$, which would then converge to a finite value, as in the TLS model.

Yet, elementary excitations deform the solid matrix, resulting in long-range elastic interactions, which would lead to a more accurate representation of the form (see, e.g., Ref. 73 and references therein)

$$V(\{x_i\}) = \sum_{i=1}^{K} v_i(x_i) - \sum_{i<j} J_{ij}x_i x_j. \tag{A3}$$

For weak enough coupling J_{ij}, the system still has $N_{IS} = 2^K$ local minima, but the DW profile of a single elementary excitation now depends on the state of all the other excitations in the system. As a result, the MEP path connecting a given pair of ISs is not necessarily decomposed into elementary transitions, and the number of DWs can be as large as $N_{DW} \sim N_{IS}^2$. Depending on the nature of elementary excitations and their interactions, one would then observe $\log N_{IS} \lesssim N_{DW} \lesssim N_{IS}^2$ and, thus, very different large scale behavior of the ratio N_{DW}/N_{IS}. Extracting the relevant elementary excitations in this situation will obviously be cumbersome.

We can tentatively interpret the stability dependence of our numerical data as a smooth crossover between interacting DWs for poorly stable glasses with large concentrations of excitations to the non-interacting ones in stable glasses where excitations become more dilute.
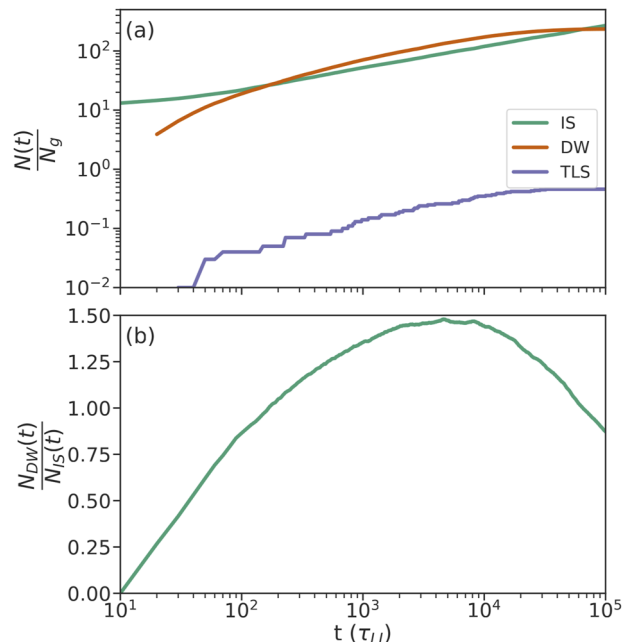
APPENDIX B: DATA FOR POLYDISPERSE SOFT SPHERES

In Fig. 11, we show data for the scaling of inherent structures and DW numbers with time for the polydisperse soft-sphere glasses studied in Ref. 21. We can see that the number of ISs grows as a power-law, with scaling exponents changing from 0.65 to 0.17 when increasing the glass stability, which is qualitatively similar to the scaling of $N_{IS}(t)$ in TLJ glasses, shown in Fig. 3(b). These exponents seem compatible with those obtained for the TLJ system.

In Fig. 12, we show the number of detected DWs as a function of time for PSS glasses. The number of DWs grows slower than the number of IS, and scaling seems slower than a power-law. All these features are the same as those observed for TLJ glasses, as shown in Fig. 4. A significant difference, however, is that at a similar glass
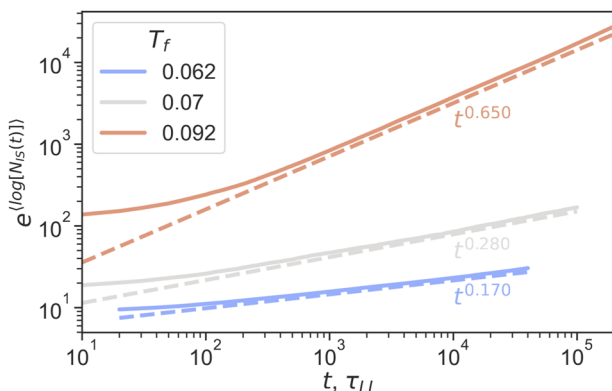
FIG. 12. Landscape exploration of polydisperse soft spheres prepared at $T_f = 0.07$. (a) Number of minima (green), double-wells (orange), and TLS (purple) sampled as a function of time. (b) Ratio of the number of DWs to the number of ISs as a function of time. The two panels share the horizontal axis.

stability and length of sampling, there are significantly more DWs per IS in the PSS model.
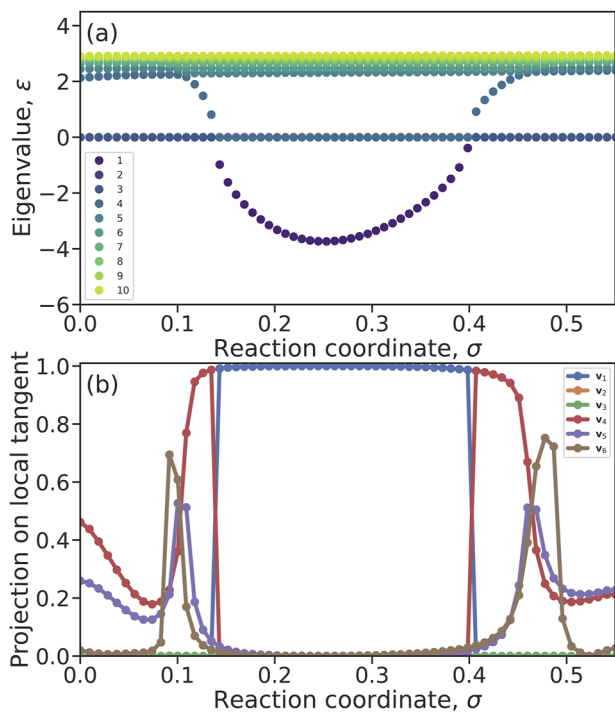
APPENDIX C: RELATIONSHIP BETWEEN THE HESSIAN AND THE MINIMUM-ENERGY PATH

We have studied the eigenvectors and eigenvalues of the Hessian for configurations along the MEP, and these are shown in Fig. 13. We find that a single eigenvalue (the lowest one) becomes negative along the MEP, indicating a first-order saddle point. Only several of the lowest frequencies change appreciably along the MEP. We also projected the first six eigenvector tangent to the MEP, and we find that the lowest mode contributes the most along the path, while contributions from several others become important only when approaching the minima.

This validates the picture of a network of minima where each pair that corresponds to a TLS is connected by a 1D path, the MEP. Orthogonal to this path, the dynamics is quasi-harmonic and is determined by a set of frequencies that are nearly independent of the reaction coordinate.

APPENDIX D: EUCLIDEAN DISTANCE BETWEEN MINIMA AND QUANTUM SPLITTING

The Euclidean distance between minima is a key quantity for tunneling DWs as it is strongly related to the tunneling rate. The scatter plot of Euclidean distance d vs the quantum splitting E is shown in Fig. 14. The Euclidean distance between ISs tends to be larger at higher T_f.

FIG. 11. Number of ISs per glass averaged geometrically averaged over all glasses for polydisperse soft spheres. Dashed lines are guides for the eye, showing power-law scaling $\sim t^\beta$, with $\beta = 0.17, 0.28, 0.65$ for $T_f = 0.062, 0.07, 0.092$, respectively.

FIG. 13. Eigenvalues and eigenvectors of the Hessian along the MEP of a typical TLS. (a) The first ten eigenvalues (in units of ε) along the MEP; the lowest eigenvalue is shown in *purple*, while the tenth mode is shown in *yellow*. (b) Projection of the first six eigenvectors on the local tangent to the MEP. The first eigenvector is shown in *blue*, while the next are shown in *orange*, *green*, *red*, *purple*, and *brown*, respectively.
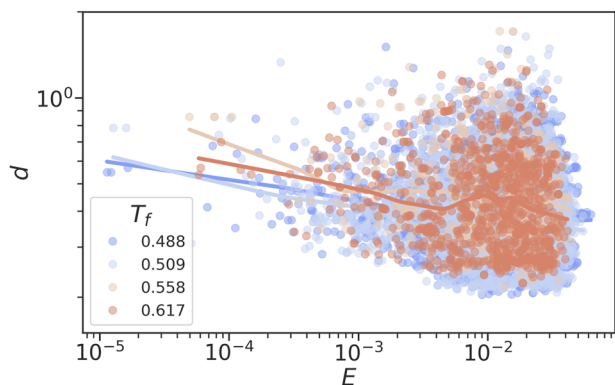
FIG. 14. Euclidean distance d vs splitting E. Colors code for different preparation temperatures T_f. Average values of d at a given E are shown as a solid line.

REFERENCES

[1]P. W. Anderson, B. I. Halperin, and C. M. Varma, "Anomalous low-temperature thermal properties of glasses and spin glasses," Philos. Mag. **25**, 1–9 (1972).

[2]W. A. Phillips, "Two-level states in glasses," Rep. Prog. Phys. **50**, 1657–1708 (1987).

[3]M. A. Ramos and U. Buchenau, "Low-temperature thermal conductivity of glasses within the soft-potential model," Phys. Rev. B **55**, 5749–5754 (1997).

[4]R. C. Zeller and R. O. Pohl, "Thermal conductivity and specific heat of noncrystalline solids," Phys. Rev. B **4**, 2029–2041 (1971).

[5]V. Lubchenko and P. G. Wolynes, "The origin of the boson peak and thermal conductivity plateau in low-temperature glasses," Proc. Natl. Acad. Sci. U. S. A. **100**, 1515–1518 (2003).

[6]*Tunneling Systems in Amorphous and Crystalline Solids*, edited by P. Esquinazi (Springer, Berlin, Heidelberg, 1998).

[7]U. Buchenau, G. D'Angelo, G. Carini, X. Liu, and M. A. Ramos, "Sound absorption in glasses," Rev. Phys. **9**, 100078 (2022).

[8]V. Lubchenko and P. G. Wolynes, "Intrinsic quantum excitations of low temperature glasses," Phys. Rev. Lett. **87**, 195901 (2001).

[9]A. J. Leggett and D. C. Vural, "'Tunneling two-level systems' model of the low-temperature properties of glasses: Are 'smoking-gun' tests possible?," J. Phys. Chem. B **117**, 12966–12971 (2013).

[10]A. L. Burin and Y. Kagan, "On the nature of the universal properties of amorphous solids," Phys. Lett. A **215**, 191–196 (1996).

[11]D. Zhou and A. J. Leggett, "Random nonlinear infinite-level-system model for amorphous solid phonon echo and saturation phenomena," arXiv:1510.05538 (2015).

[12]D. Zhou, "Universal ratio of TTLS-phonon coupling constants in low-temperature amorphous solids," J. Phys.: Condens. Matter **32**, 055704 (2019).

[13]H. M. Carruzzo and C. C. Yu, "Why phonon scattering in glasses is universally small at low temperatures," Phys. Rev. Lett. **124**, 075902 (2020).

[14]H. M. Carruzzo, A. Bilmes, J. Lisenfeld, Z. Yu, B. Wang, Z. Wan, J. R. Schmidt, and C. C. Yu, "Distribution of two-level system couplings to strain and electric fields in glasses at low temperatures," Phys. Rev. B **104**, 134203 (2021).

[15]C. Artiaco, F. Balducci, and A. Scardicchio, "Signatures of many-body localization in the dynamics of two-level systems in glasses," Phys. Rev. B **103**, 214205 (2021).

[16]V. Lubchenko and P. G. Wolynes, "The microscopic quantum theory of low temperature amorphous solids," in *Advances in Chemical Physics*, edited by S. A. Rice (John Wiley & Sons, Hoboken, NJ, 2008), pp. 95–206.

[17]A. Heuer and R. J. Silbey, "Microscopic description of tunneling systems in a structural model glass," Phys. Rev. Lett. **70**, 3911–3914 (1993).

[18]F. Demichelis, G. Viliani, and G. Ruocco, "Properties of the double well potential and relaxation processes in a model glass," PhysChemComm **2**, 20–23 (1999).

[19]J. Reinisch and A. Heuer, "How cooperative are the dynamics in tunneling systems? A computer study for an atomic model glass," J. Low Temp. Phys. **137**, 267–287 (2004).

[20]T. Damart and D. Rodney, "Atomistic study of two-level systems in amorphous silica," Phys. Rev. B **97**, 014201 (2018).

[21]D. Khomenko, C. Scalliet, L. Berthier, D. R. Reichman, and F. Zamponi, "Depletion of two-level systems in ultrastable computer-generated glasses," Phys. Rev. Lett. **124**, 225901 (2020).

[22]A. Kumar, I. Procaccia, and M. Singh, "Density of quasi-localized modes in athermal glasses," Europhys. Lett. **135**, 66001 (2021).

[23]C. Müller, J. H. Cole, and J. Lisenfeld, "Towards understanding two-level-systems in amorphous solids: Insights from quantum circuits," Rep. Prog. Phys. **82**, 124501 (2019).

[24]R. Birney, J. Steinlechner, Z. Tornasi, S. MacFoy, D. Vine, A. S. Bell, D. Gibson, J. Hough, S. Rowan, P. Sortais, S. Sproules, S. Tait, I. W. Martin, and S. Reid, "Amorphous silicon with extremely low absorption: Beating thermal noise in gravitational astronomy," Phys. Rev. Lett. **121**, 191101 (2018).

[25]J. Steinlechner, I. W. Martin, A. S. Bell, J. Hough, M. Fletcher, P. G. Murray, R. Robie, S. Rowan, and R. Schnabel, "Silicon-based optical mirror coatings for ultrahigh precision metrology and sensing," Phys. Rev. Lett. **120**, 263602 (2018).

[26]A. Q. Tool, "Relation between inelastic deformability and thermal expansion of glass in its annealing range," J. Am. Ceram. Soc. **29**, 240–253 (1946).

[27]D. R. Queen, X. Liu, J. Karel, T. H. Metcalf, and F. Hellman, "Excess specific heat in evaporated amorphous silicon," Phys. Rev. Lett. **110**, 135901 (2013).

[28]T. Pérez-Castañeda, C. Rodríguez-Tinoco, J. Rodríguez-Viejo, and M. A. Ramos, "Suppression of tunneling two-level systems in ultrastable glasses of indomethacin," Proc. Natl. Acad. Sci. U. S. A. **111**, 11275–11280 (2014).

[29] A. Ninarello, L. Berthier, and D. Coslovich, "Models and algorithms for the next generation of glass transition studies," Phys. Rev. X 7, 021039 (2017).

[30] L. Berthier and D. R. Reichman, "Modern computational studies of the glass transition," arXiv:2208.02206 (2022).

[31] A. D. S. Parmar, M. Ozawa, and L. Berthier, "Ultrastable metallic glasses in silico," Phys. Rev. Lett. 125, 085505 (2020).

[32] J. F. Berret and M. Meißner, "How universal are the low temperature acoustic properties of glasses?," Z. Phys. B: Condens. Matter 70, 65–72 (1988).

[33] W. Ji, "Toward understanding the depletion of two-level systems in ultrastable glasses," arXiv:2112.10105 (2021).

[34] B. Doliwa and A. Heuer, "Energy barriers and activated dynamics in a supercooled Lennard-Jones liquid," Phys. Rev. E 67, 031506 (2003).

[35] R. A. Denny, D. R. Reichman, and J. P. Bouchaud, "Trap models and slow dynamics in supercooled liquids," Phys. Rev. Lett. 90, 025503 (2003).

[36] F. H. Stillinger and T. A. Weber, "Hidden structure in liquids," Phys. Rev. A 25, 978 (1982).

[37] F. Sciortino, "Potential energy landscape description of supercooled liquids and glasses," J. Stat. Mech.: Theory Exp. 2005, P05015.

[38] A. Heuer, "Exploring the potential energy landscape of glass-forming systems: From inherent structures via metabasins to macroscopic transport," J. Phys.: Condens. Matter 20, 373101 (2008).

[39] H. Jónsson, G. Mills, and K. W. Jacobsen, "Nudged elastic band method for finding minimum energy paths of transitions," in Classical and Quantum Dynamics in Condensed Phase Simulations, edited by B. J. Berne, G. Ciccotti, and D. F. Coker (World Scientific, Singapore, 1998).

[40] G. Henkelman and H. Jónsson, "Improved tangent estimate in the nudged elastic band method for finding minimum energy paths and saddle points," J. Chem. Phys. 113, 9978–9985 (2000).

[41] M. T. Loponen, R. C. Dynes, V. Narayanamurti, and J. P. Garno, "Measurements of the time-dependent specific heat of amorphous materials," Phys. Rev. B 25, 1161 (1982).

[42] W. Gutiérrez, S. Karmakar, Y. G. Pollack, and I. Procaccia, "The static lengthscale characterizing the glass transition at lower temperatures," Europhys. Lett. 111, 56009 (2015).

[43] W. Kob and H. C. Andersen, "Testing mode-coupling theory for a supercooled binary Lennard-Jones mixture I: The van Hove correlation function," Phys. Rev. E 51, 4626–4641 (1995).

[44] S. Sastry, "Liquid limits: Glass transition and liquid-gas spinodal boundaries of metastable liquids," Phys. Rev. Lett. 85, 590–593 (2000).

[45] V. Testard, L. Berthier, and W. Kob, "Influence of the glass transition on the liquid-gas spinodal decomposition," Phys. Rev. Lett. 106, 125702 (2011).

[46] S. Plimpton, "Fast parallel algorithms for short-range molecular dynamics," J. Comput. Phys. 117, 1–19 (1995).

[47] L. Berthier, E. Flenner, C. J. Fullerton, C. Scalliet, and M. Singh, "Efficient swap algorithms for molecular dynamics simulations of equilibrium supercooled liquids," J. Stat. Mech.: Theory Exp. 2019, 064004.

[48] M. D. Ediger, C. A. Angell, and S. R. Nagel, "Supercooled liquids and glasses," J. Phys. Chem. 100, 13200–13212 (1996).

[49] Y. S. Elmatad, D. Chandler, and J. P. Garrahan, "Corresponding states of structural glass formers. II," J. Phys. Chem. B 114, 17113–17119 (2010).

[50] D. Frenkel and B. Smit, Understanding Molecular Simulation: From Algorithms to Applications (Academic Press, 1996).

[51] W. E, W. Ren, and E. Vanden-Eijnden, "String method for the study of rare events," Phys. Rev. B 66, 052301 (2002).

[52] E. Bitzek, P. Koskinen, F. Gähler, M. Moseler, and P. Gumbsch, "Structural relaxation made simple," Phys. Rev. Lett. 97, 170201 (2006).

[53] J. Guénolé, W. G. Nöhring, A. Vaid, F. Houllé, Z. Xie, A. Prakash, and E. Bitzek, "Assessment and optimization of the fast inertial relaxation engine (FIRE) for energy minimization in atomistic simulations and its implementation in LAMMPS," Comput. Mater. Sci. 175, 109584 (2020).

[54] W. E, W. Ren, and E. Vanden-Eijnden, "Simplified and improved string method for computing the minimum energy paths in barrier-crossing events," J. Chem. Phys. 126, 164103 (2007).

[55] G. Henkelman, B. P. Uberuaga, and H. Jónsson, "A climbing image nudged elastic band method for finding saddle points and minimum energy paths," J. Chem. Phys. 113, 9901–9904 (2000).

[56] C. Scalliet, L. Berthier, and F. Zamponi, "Nature of excitations and defects in structural glasses," Nat. Commun. 10, 5102 (2019).

[57] Q. Liao and L. Berthier, "Hierarchical landscape of hard disk glasses," Phys. Rev. X 9, 011049 (2019).

[58] C. Artiaco, P. Baldan, and G. Parisi, "Exploratory study of the glassy landscape near jamming," Phys. Rev. E 101, 052605 (2020).

[59] G. H. Vineyard, "Frequency factors and isotope effects in solid state rate processes," J. Phys. Chem. Solids 3, 121–127 (1957).

[60] R. B. Lehoucq, D. C. Sorensen, and C. Yang, ARPACK Users' Guide: Solution of Large-Scale Eigenvalue Problems with Implicitly Restarted Arnoldi Methods (Society for Industrial and Applied Mathematics, 1998).

[61] G. Frossati, J. l. Gilchrist, J. C. Lasjaunias, and W. Meyer, "Spectrum of low-energy dipolar states in hydrated vitreous silica," J. Phys. C: Solid State Phys. 10, L515 (1977).

[62] V. Jakšić and J. Segert, "On the Landau–Zener formula for two-level systems," J. Math. Phys. 34, 2807–2820 (1993).

[63] T. Vegge, J. P. Sethna, S.-A. Cheong, K. W. Jacobsen, C. R. Myers, and D. C. Ralph, "Calculation of quantum tunneling for a spatially extended defect: The dislocation kink in copper has a low effective mass," Phys. Rev. Lett. 86, 1546–1549 (2001).

[64] C. Lévesque, S. Roorda, F. Schiettekatte, and N. Mousseau, "Internal mechanical dissipation mechanisms in amorphous silicon," Phys. Rev. Mater. 6, 123604 (2022); arXiv:2209.02342 [cond-mat].

[65] M. Ozawa, C. Scalliet, A. Ninarello, and L. Berthier, "Does the Adam-Gibbs relation hold in simulated supercooled liquids?," J. Chem. Phys. 151, 084504 (2019).

[66] C. Scalliet, B. Guiselin, and L. Berthier, "Thirty milliseconds in the life of a supercooled liquid," Phys. Rev. X 12, 041028 (2022); arXiv:2207.00491.

[67] T. A. Weber and F. H. Stillinger, "Local order and structural transitions in amorphous metal-metalloid alloys," Phys. Rev. B 31, 1954–1963 (1985).

[68] K. González-López, M. Shivam, Y. Zheng, M. P. Ciamarra, and E. Lerner, "Mechanical disorder of sticky-sphere glasses. I. Effect of attractive interactions," Phys. Rev. E 103, 022605 (2021).

[69] L. Wang, A. Ninarello, P. Guan, L. Berthier, G. Szamel, and E. Flenner, "Low-frequency vibrational modes of stable glasses," Nat. Commun. 10, 26 (2019).

[70] G. Kapteijns, E. Bouchbinder, and E. Lerner, "Universal nonphononic density of states in 2D, 3D, and 4D glasses," Phys. Rev. Lett. 121, 055501 (2018).

[71] L. Wang, L. Fu, and Y. Nie, "Density of states below the first sound mode in 3D glasses," J. Chem. Phys. 157, 074502 (2022); arXiv:2206.05270.

[72] D. Khomenko, D. R. Reichman, and F. Zamponi, "Relationship between two-level systems and quasilocalized normal modes in glasses," Phys. Rev. Mater. 5, 055602 (2021).

[73] G. Folena and P. Urbani, "Marginal stability of soft anharmonic mean field spin glasses," J. Stat. Mech.: Theory Exp. 2022, 053301.

[74] L. Berthier, "Self-induced heterogeneity in deeply supercooled liquids," Phys. Rev. Lett. 127, 088002 (2021).

[75] M. Marchi and D. Chandler, "Path-integral calculation of the tunnel splitting in aqueous ferrous–ferric electron transfer," J. Chem. Phys. 95, 889–894 (1991).

[76] C. L. Vaillant, D. J. Wales, and S. C. Althorpe, "Tunneling splittings from path-integral molecular dynamics using a Langevin thermostat," J. Chem. Phys. 148, 234102 (2018); arXiv:1803.04433.